Journal of Thermal Analysis and Calorimetry, Vol. 94 (2008) 2, 499–505

THERMAL STABILITY OF HEXAGONAL TUNGSTEN TRIOXIDE IN AIR

I. M. Szilágyi[1*], *Judit Pfeifer*[2], *C. Balázsi*[2], *A. L. Tóth*[2], *Katalin Varga-Josepovits*[3], *J. Madarász*[4] *and G. Pokol*[4]

[1]Materials Structure and Modeling Research Group of the Hungarian Academy of Sciences, Budapest University of Technology and Economics, Department of Inorganic and Analytical Chemistry, 1111 Budapest, Szt. Gellért tér 4., Hungary
[2]Ceramics and Nanocomposites Laboratory, Research Institute for Technical Physics and Materials Science, 1121 Budapest Konkoly-Thege út 29–33, Hungary
[3]Department of Atomic Physics, Budapest University of Technology and Economics, 1111 Budapest, Budafoki út 8, Hungary
[4]Department of Inorganic and Analytical Chemistry, Budapest University of Technology and Economics, 1111 Budapest Szt. Gellért tér 4, Hungary

We studied the thermal stability of different hexagonal tungsten trioxide, h-WO_3 samples, which were prepared either by annealing hexagonal ammonium tungsten bronze, $(NH_4)_{0.33-x}WO_{3-y}$, or by soft chemical synthesis from Na_2WO_4. The structure and composition of the samples were studied by powder XRD, SEM-EDX, XPS and ^{1}H-MAS NMR. The thermal properties were investigated by simultaneous TG/DTA, on-line evolved gas analysis (TG/DTA-MS), SEM and in situ powder XRD. The preparative routes influenced the thermal properties of h-WO_3 samples, i.e. the course of water release, the exothermic collapse of the hexagonal framework and the phase transformations were all affected.

Keywords: *evolved gas analysis by MS, hexagonal tungsten oxide, in situ studies, simultaneous TG/DTA, X-ray diffraction*

Introduction

For applications in photoelectrochromical cells and chromogenic (electro-, photo- and thermochromic) devices [1–11], gas sensors [12–17] and catalysts [18–21], tungsten oxides have attracted much attention in the past decades. Hexagonal tungsten trioxide, h-WO_3 is one of the most researched tungsten oxides due to its open-tunnel structure and intercalation chemistry [22–24]. It has been prepared in several ways: by dehydration of tungsten oxide hydrates [24, 25], by wet chemical synthesis using various precursors [26, 27], by thermal oxidation of tungsten metal [28], by thermal or wet chemical oxidation of hexagonal ammonium tungsten bronze [22, 29–31], by ion exchanging template ions from hexagonal tungsten bronze [32] or by spray pyrolysis [10].

The thermal stability of h-WO_3 is important in the previously mentioned application fields, especially there, where h-WO_3 is used at elevated temperatures, e.g. by gas sensors. The thermal behaviour of the title compound has already been studied by thermogravimetry (TG) [24], differential scanning calorimetry (DSC) and differential thermal analysis (DTA) [7, 29, 33], X-ray powder diffraction (XRD) [34–36], transmission and scanning electron microscopy (TEM and SEM) [36, 37], Raman [7] and FTIR spectroscopy [34]. The results have showed that h-WO_3 transforms into monoclinic (m-) WO_3 in an exothermic reaction between 250–500°C. Other studies on m-WO_3 have revealed that m-WO_3 transforms reversibly into tetragonal (t-) WO_3 between 700–800°C [1, 38].

The different preparative routes result in different morphology and different composition with varying amounts of residual elements, and these might affect the thermal properties of h-WO_3. Therefore it seemed advisable to compare the thermal behavior of differently prepared h-WO_3 samples. This was also encouraged by the lack of evolved gas analytical (EGA) studies on h-WO_3.

Thus, here we present a comparison of the thermal stability of different h-WO_3 samples, which were prepared either by thermal oxidation of hexagonal ammonium tungsten bronze (HATB), $(NH_4)_{0.33-x}WO_{3-y}$ (Sample 1), or by soft chemical synthesis, i.e. acidification of Na_2WO_4 solution followed by washing and hydrothermal treatment (Samples 2, 2a, 2b). Recently the authors managed to prepare highly crystalline, monophase HATB, $(NH_4)_{0.07}(NH_3)_{0.04}(H_2O)_{0.09}WO_{2.95}$ by heating ammonium paratungstate tetrahydrate, $(NH_4)_{10}[H_2W_{12}O_{42}]\cdot 4H_2O$ in H_2 for 6 h at 400°C [39]. This gave us chance to prepare good quality h-WO_3 by oxidizing the highly crystalline HATB starting material in air. On the other hand, the authors also had experience with

* Author for correspondence: imre.szilagyi@mail.bme.hu

1388–6150/$20.00

Akadémiai Kiadó, Budapest, Hungary
Springer, Dordrecht, The Netherlands

the soft chemical synthesis of h-WO_3 from Na_2WO_4 [17, 24, 40, 41].

The structure and composition of the samples was studied by XRD, scanning electron microscopy with energy dispersive X-ray analysis (SEM-EDX), X-ray photoelectron spectroscopy (XPS) and solid-state ^{1}H-MAS (Magic Angle Spinning) NMR spectroscopy. The thermal behavior of hexagonal tungsten oxides was investigated by simultaneous TG/DTA, on-line coupled evolved gas analysis with mass spectrometer (TG/DTA-MS), SEM and in situ high temperature X-ray powder diffraction (HT-XRD).

The two types of samples had differences in morphology and composition, i.e. (1) consisted of μm scale blocks of nanoparticles and contained NH_4^+ ion residues and (2) had nm scale particles and contained Na^+ ion residues. The differences in morphology and composition resulted in different thermal properties.

Experimental

Sample of h-WO_3 (1) was prepared by heating highly crystalline, monophase hexagonal ammonium tungsten bronze (HATB), $(NH_4)_{0.07}(NH_3)_{0.04}(H_2O)_{0.09}WO_{2.95}$ [39] in air (15 L h^{-1}) at 10°C min^{-1} to 470°C and then keeping it there isothermally for 3 min in an open aluminium crucible in a DuPont 910 DSC instrument.

Samples of h-WO_3 (2, 2a, 2b) were prepared by soft chemical synthesis, i.e. by acidification of Na_2WO_4 solution followed by washing and hydrothermal treatment of the precipitate [24, 40, 41]. By this route first $WO_3 \cdot 0.33H_2O$ is prepared from Na_2WO_4 in aqueous phase, then the oxide hydrate transforms into h-WO_3. 2 was made up of monophase h-WO_3. 2a contained some $WO_3 \cdot 0.33H_2O$ traces from the precursor. 2b contained high amount of residual sodium, ca. 1.2 mass% in the bulk and ca. 2.3 mass% on the surface. 2a and 2b were included in the studies, because their composition showed deviations from standard h-WO_3 samples. Therefore by these samples we could check the effect of different compositions on the thermal properties of h-WO_3.

The sodium content of 2b was measured by both X-ray photoelectron spectroscopy (XPS) and energy dispersive X-ray analysis (within a scanning electron microscope) (SEM-EDX). XPS data were collected by a VG Microtech instrument consisting of a XR3E2 X-ray source, a twin anode (MgK_α and AlK_α) and a CLAM 2 hemispherical analyser using MgK_α radiation. SEM-EDX measurements were performed in a Röntec QuanTAX energy dispersive microanalyser system.

The ammonium ion and ammonia molecule content of 1 could only be measured by ^{1}H-MAS-NMR spectroscopy; by XPS or FTIR spectroscopy we could not detect these species [39]. ^{1}H-MAS-NMR experiments were carried out on a VARIAN NMR SYSTEM spectrometer (600 MHz for ^{1}H) using a 3.2 mm HXY VARIAN/Chemagnetics probe. ^{1}H chemical shifts were referenced to adamantane (δ_{1H}=0 ppm). All spectra were recorded under the same experimental conditions. 16 transients were acquired at 12 kHz spinning rate and a recycle delay of 20 s was used. Background suppression DEPTH [42] was employed to remove signals from the probe. The composition of precursor HATB was determined earlier by chemical analysis, XPS and ^{1}H-MAS-NMR spectroscopy [39], and in HATB the NH_4^+/NH_3 amount was 0.55 and 0.32 mass%, respectively. Now we measured the ^{1}H-MAS-NMR spectra of both HATB and **1**, and by comparing the normalized signals of NH_4^+ and NH_3 peaks [39], we could estimate semiquantitatively the NH_4^+/NH_3 amount of 1, which was ca. 0.11 and 0.04 mass%, respectively.

Powder X-ray diffraction (XRD) pattern of 1 was measured by a PANalytical X'pert Pro MPD X-ray diffractometer equipped with an X'Celerator detector using CuK_α radiation. XRD patterns of 2, 2a and 2b were recorded by a Bruker AXS D8 Discover X-ray diffractometer using CuK_α radiation.

A LEO-1550 FEG SEM instrument was used during the SEM characterisation of 1, 2, 2a, 2b and their decomposition products.

During the evolved gas analytical (TG/DTA-MS) measurements of 1, 2, 2a and 2b, open platinum crucible, a heating rate of 10°C min^{-1}, sample sizes of 30–100 mg and flowing air (130 mL min^{-1}) were used. The TG/DTA-MS apparatus consisted of an STD 2960 Simultaneous DTA/TGA (TA Instruments Inc.) thermal analyzer and a Thermostar GSD 200 (Balzers Instruments) quadrupole mass spectrometer. The details of the TG/DTA-MS setup are discussed elsewhere [43, 44].

In situ high temperature X-ray diffraction (HT-XRD) patterns of 1 and 2 were collected by a PANalytical X'pert Pro MPD X-ray diffractometer equipped with an X'Celerator detector and an Anton Paar HTK-2000 high temperature XRD chamber using CuK_α radiation. The scanning time was ca. 3 min for each pattern. HT-XRD experiments were performed in static air using 10°C min^{-1} heating rate between XRD measurements.

Results and discussion

Characterization of h-WO_3 samples

The difference in the composition of the h-WO_3 samples was obvious. Besides tungsten and oxygen, 1 contained little amounts of ammonium ions and am-

monia molecules (0.11 and 0.04 mass%, respectively), which had remained from the parent hexagonal ammonium tungsten bronze phase. 2 and 2a contained certain amount (0.02–0.1 mass%) of sodium, which was necessary for the formation of h-WO_3 during the soft chemical synthesis [17, 24, 40, 41]. In 2b the amount of sodium was relatively high. By SEM-EDX it was determined to be ca. 1.2 mass%, and by XPS it was found to be ca. 2.3 mass%. The two methods complement each other: in SEM-EDX the information depth of the analysis is 400–500 nm, while in XPS it is only about 5–10 nm, thus SEM-EDX gives roughly the bulk concentration and XPS gives the surface concentration of the elements.

The different preparative routes strongly affected the morphology. 1 consisted of 1–80 μm yellow particles, which were cracked. Under higher magnification we found that actually they were built up of 50–100 nm aggregated particles (Figs 1a and b). 2, 2a and 2b were greyish-white coloured and they consisted of 20–30 nm thick platelets and rods, which aggregated into 1–2 μm particles (Fig. 1c). The different color of 1 and 2, 2a, 2b suggests different electronic structure, which might affect applications. The morphology of 2, 2a and 2b showed no significant differences, thus only the SEM image of sample (2a) is shown in Fig. 1c.

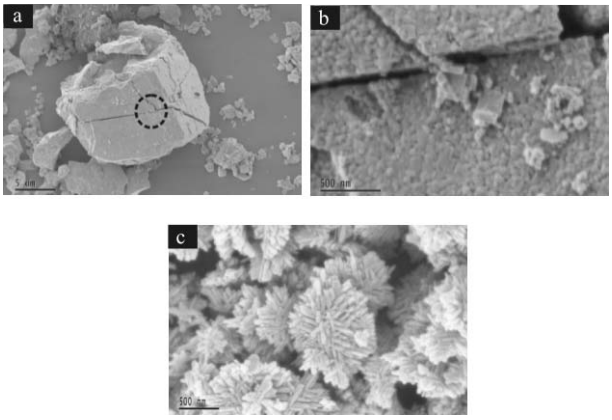

Fig. 1 SEM images of a – h-WO_3 (1) at lower (10k) magnification, b – h-WO_3 (1) at higher (150k) magnification; the black dashed circle in the middle of a – shows the area from where b – was taken, c – h-WO_3 (2a)

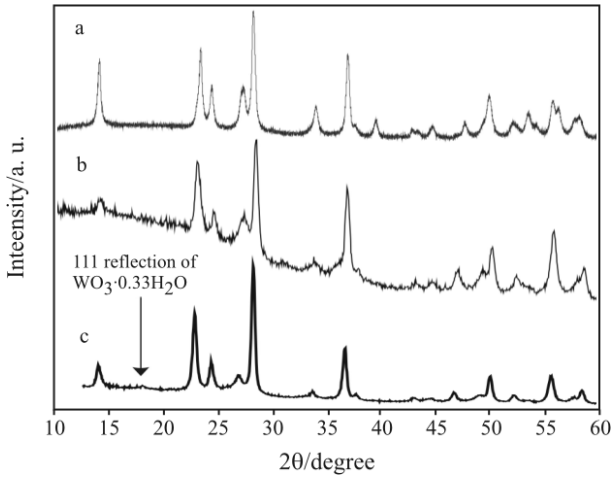

Fig. 2 XRD patterns of a – h-WO_3 (1), b – h-WO_3 (2) and c – h-WO_3 (2a)

There were only small differences in the XRD patterns of 1 and 2 (Fig. 2), and they were both identified as pure h-WO_3 (ICDD 85-2460 and 33-1387). As already discussed, $WO_3 \cdot 0.33H_2O$ (ICDD 35-0270) was also detected in 2a (Fig. 2). 2b had identical XRD pattern as 2, and thus it is not shown in Fig. 2.

Thermal behaviour of 1

The TG/DTA and evolved gas analytical (TG/DTA-MS) curves of 1 are presented in Fig. 3. The evolved gas analytical study showed only the evolution of water. Though 1 contained traces of ammonium ions and ammonia molecules, their amount was so small that their release could not be detected well with the TG/DTA-MS system. The HT-XRD patterns of 1 are shown in Fig. 4. The SEM image of the decomposition product of 1 at 900°C is presented in Fig. 5a.

According to the thermoanalytical curves, up to 200°C adsorbed and chemisorbed water were released in two overlapping endothermic reactions. Between 200–400°C water release continued, but here no significant heat effect was observed and the amount of evolved water was much smaller than below 200°C. Based on the XRD patterns, the starting h-WO_3 structure remained nearly the same up to 450°C.

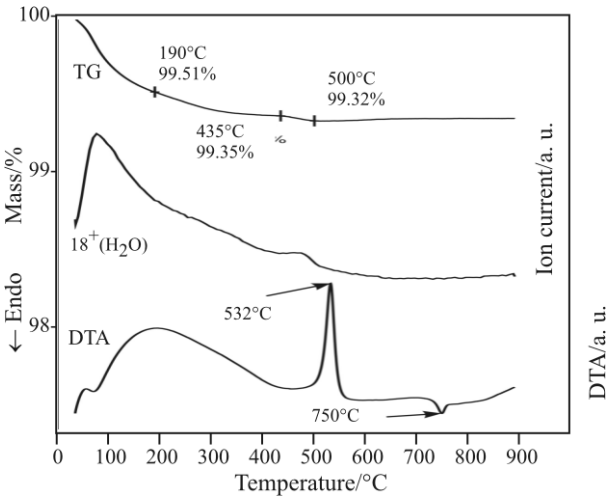

Fig. 3 Simultaneous TG/DTA and evolved gas analytical curves of h-WO_3 (1) measured in air (130 mL min^{-1}, 10°C min^{-1}, open Pt crucible, 102.4 mg)

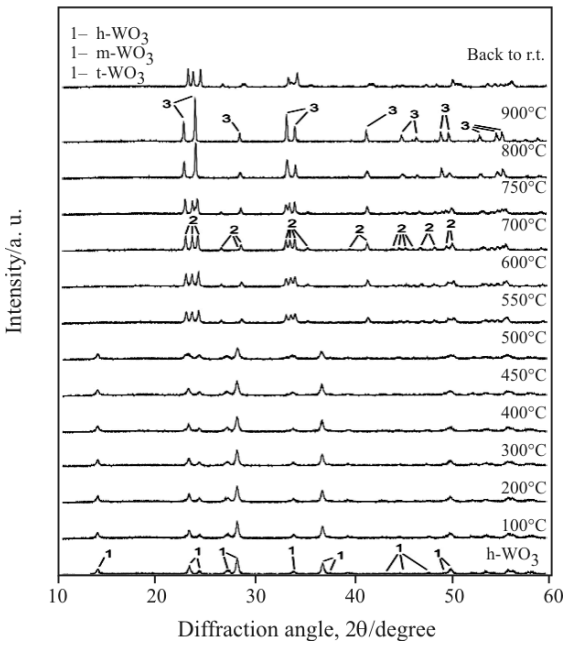

Fig. 4 In situ HT-XRD patterns of h-WO_3 (1) in static air recorded from *r.t.* to 900°C

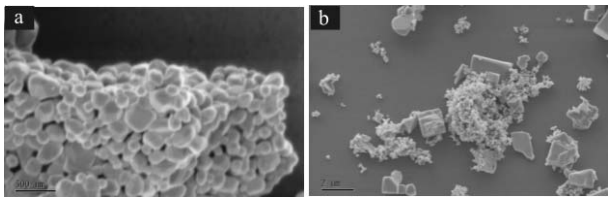

Fig. 5 SEM images of decomposition products at 900°C in air of a – h-WO_3 (1) and b – h-WO_3 (2)

Between 450–500°C another water release step took place. At 500°C the reflections of h-WO_3 became more diffuse in the XRD patterns. Then between 500–550°C the hexagonal structure collapsed in an exothermic reaction, and transformed irreversibly into monoclinic (m-) WO_3 (ICDD 43-1035). Since the h-WO_3 structure is metastable, it is easy to understand that its transformation into the more stable m-WO_3 is an exothermic reaction – as was shown by our measurements and previous results [29].

The m-WO_3 phase was stable up to 700°C. Around 750°C it transformed into tetragonal (t-) WO_3 (ICDD 85-0807) in a reversible endothermic reaction. At 750°C the HT-XRD analysis showed a mixture of m- and t-WO_3, while by 800°C only t-WO_3 was present. The well known reversibility [1, 38] of the m- and t-WO_3 transformation is reflected also by that when the sample was cooling (not shown on Fig. 3), there was an exothermic DTA peak where t-WO_3 transformed back into m-WO_3. At room temperature (*r.t.*) only m-WO_3 was observed.

The SEM image of the decomposition product of 1 at 900°C showed 100–500 nm particles instead of the 50–100 nm particles observed in the starting material. The crystallization of the more stable m-WO_3 from h-WO_3 and the further annealing of m-WO_3 are probably responsible for the growth of the particle size.

Thermal behaviour of 2

The TG/DTA and evolved gas analytical (TG/DTA-MS) curves of 2 are presented in Fig. 6. The evolved gas analytical study showed only the evolution of water. The HT-XRD patterns of 2 are shown in Fig. 7. The SEM image of the decomposition product of 2 at 900°C is presented in Fig. 5b.

When heating 2 at first adsorbed and chemisorbed water were released in two overlapping endothermic reactions. But here this stage extended up to 250–300°C, and the mass loss corresponding to adsorbed and chemisorbed water was also greater (1.61% at 250°C) than in the case of 1 (0.49% at 190°C). The greater mass loss should be due to the

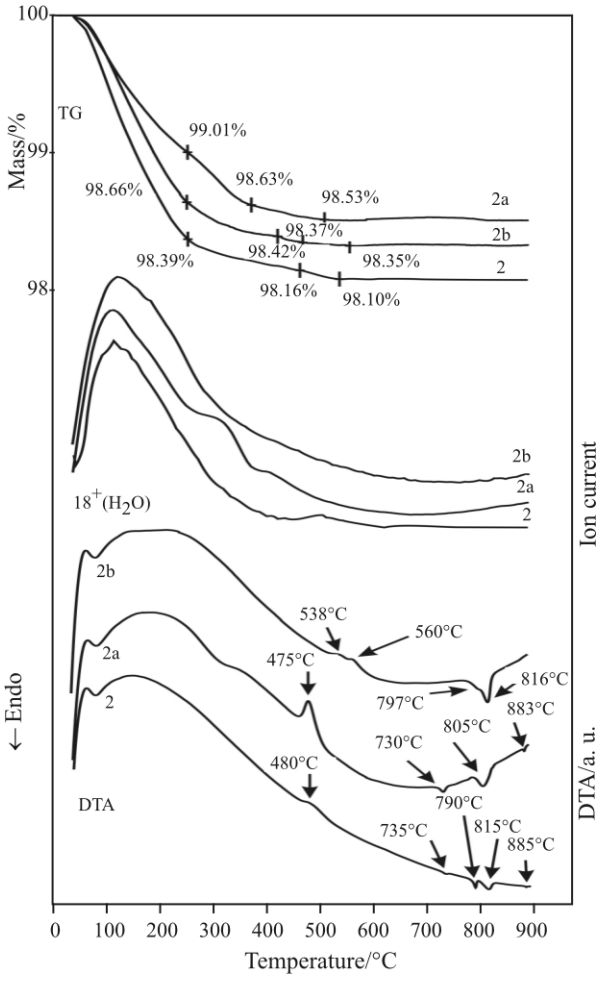

Fig. 6 Simultaneous TG/DTA and evolved gas analytical curves of h-WO_3 (2), (2a) and (2b) measured in air (130 mL min^{-1}, 10°C min^{-1}, open Pt crucible, 29.7, 40.8 and 29.8 mg, respectively)

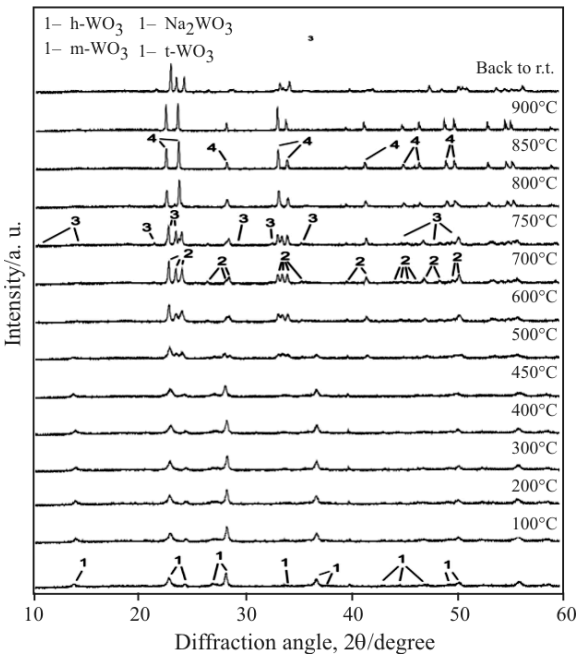

Fig. 7 In situ HT-XRD patterns of h-WO_3 (2) in static air recorded from *r.t.* to 900°C

morphology of 2, because the smaller particles of 2 have larger specific surface and hence greater amount of adsorbed and chemisorbed molecules. Between 250–450°C the water release continued, similarly as in case of 1.

Between 450–550°C the hexagonal structure collapsed, and 2 transformed irreversibly in an exothermic reaction into m-WO_3, at 50°C lower temperature than 1. This transformation was accompanied also by the release of small amount of water, similarly as for 1. The sample at 500°C contained mostly m-WO_3 and some h-WO_3. Up to this point, the thermal decomposition of 1 and 2 involved the same processes, only their dynamics was different.

When 2 was heated further, according to XRD patterns, the m-WO_3 structure was ordering, i.e. the intensity of reflections of m-WO_3 increased. Only at 700°C, a well defined m-WO_3 structure was present. Then m-WO_3 started its reversible transformation into tetragonal (t-) WO_3 between 700–750°C. At 750°C the sample still contained mainly m-WO_3 with some t-WO_3. At 800°C the main component was t-WO_3 with traces of m-WO_3, and at 850°C only t-WO_3 was detected.

2 contained sodium besides tungsten and oxygen, and after the collapse of the hexagonal framework, this sodium content was responsible for the formation of sodium tungsten oxides. The analysis of the sodium containing phases had great uncertainty. On the one hand their amount was small, on the other hand in some cases they were not well defined phases. Therefore it was difficult to match the phases, which were formed in our experiments, with the available ICDD cards. The $Na_2W_4O_{13}$ (ICDD 27-1425, 21-1667) phase was well detected, while the presence of tungsten bronzes was only guessed.

The $Na_2W_4O_{13}$ phase was observed in small amounts already at 700°C. The presence of $Na_2W_4O_{13}$ is also supported by the fact that this phase also appeared during the thermal decomposition of a tungsten sodium hydroxide, $Na_{0.4}WO_3 \cdot 0.6H_2O$ [45]. The amount of $Na_2W_4O_{13}$ increased at 750°C, then decreased at 800°C, and by 850°C it disappeared completely. But in the sample cooled back to *r.t.* it was observable again.

Between 700–900°C four endothermic heat effects were observed on the DTA curve of 2, and we suggest an explanation for them on the basis of the HT-XRD results. The $Na_2W_4O_{13}$ phase formed up to 750°C, because its amount was the largest at this temperature, so this endothermic peak at 735°C should be connected with the appearance of $Na_2W_4O_{13}$. The main part of the m- to t-WO_3 transformation took place between 750–800°C, therefore we assume that the endothermic peak at 790°C might belong to this reaction. Though, it has to be mentioned that this temperature is 40°C higher than in the case of 1.

By 850°C $Na_2W_4O_{13}$ disappeared and only t-WO_3 was detected. Since after cooling back to *r.t.* the sample contained $Na_2W_4O_{13}$ again besides m-WO_3, it means that this phase did not decompose, but melted between 800–850°C, and the endothermic heat at 815°C effect should correspond to the melting heat of the $Na_2W_4O_{13}$ phase. The SEM image of the decomposition product of 2 at 900°C also supports this idea (Fig. 5b). In this picture, the coexistence of m-WO_3 nanoparticles (small particles) and $Na_2W_4O_{13}$ microparticles (large crystals) can be seen. The solidifying of $Na_2W_4O_{13}$ from its melt explains well, how 0.5–4 μm particles could be formed from the starting 20–30 nm h-WO_3 particles.

It needs further investigation to explain the source of the tiny heat effect at 885°C. The XRD pattern at 900°C was practically the same as at 850°C. The only difference was that the CuK_{α_1} and K_{α_2} reflections became split, particularly at higher 2θ values, which showed an increase in the crystalline order.

Thermal behaviour of 2a and 2b

Due to the $WO_3 \cdot 0.33H_2O$ content of 2a and the high sodium content of 2b, a different thermal behavior was found in both cases in comparison to 2. The TG/DTA and evolved gas analytical (TG/DTA-MS) curves of 2a and 2b are presented in Fig. 5. The evolved gas analytical study showed only the evolution of water.

The additional $WO_3 \cdot 0.33H_2O$ content of 2a was responsible for the endothermic water release step between 250-370°C. Therefore thermal analysis is a good tool to check the state of the $WO_3 \cdot 1/3H_2O \rightarrow$h-$WO_3$ conversion.

By both 2 and 2b the water release ended parallel to the collapse of the hexagonal structure, similarly as in case of 1 and 2. As a significant difference this collapse occurred nearly at 100°C higher temperature in the case of 2b, compared to 2 and 2a. This should be the result of the high sodium content of 2b, which might have stabilized the crystal structure better. The exothermic DTA peak belonging to the collapse of the hexagonal structure showed an additional overlapping reaction by 2b.

Between 750–850°C there was only one endothermic DTA peak instead of two by 2a and 2b. The greater sample mass of 2a, i.e. 40 mg of 2a instead of 30 mg as of 2, and the higher Na content of 2b, i.e. larger melting heat of Na_2WO_4, might be responsible why the two endothermic peaks were not separated, but overlapped each other. In addition in the case of 2b we did not observe any endothermic DTA peak between 700–750 and 850–900°C.

Conclusions

The thermal behavior of differently prepared h-WO_3 samples was studied by on-line evolved gas analysis (TG/DTA-MS), in situ high temperature X-ray diffraction (HT-XRD) and scanning electron microscopy (SEM). Our measurements showed that the preparative routes influenced the thermal behavior of different h-WO_3 samples.

The h-WO_3 samples were prepared either by thermal oxidation of hexagonal ammonium tungsten bronze, $(NH_4)_{0.33-x}WO_{3-y}$ (Sample **1**), or by soft chemical synthesis from Na_2WO_4 (Samples 2, 2a, 2b). The two preparative routes resulted in different morphology and colour. In addition 2a contained also $WO_3 \cdot 0.33H_2O$ besides h-WO_3 and 2b had relatively high sodium content, i.e. 1.2 mass%

When heating the samples, as common feature up to 200–250°C, adsorbed and chemisorbed water, then up to 450–500°C structural water were released. The small amount of $WO_3 \cdot 0.33H_2O$ in 2a caused an additional endothermic water release step between 250–370°C. Therefore thermal analysis is a good tool to check the state of the $WO_3 \cdot 0.33H_2O \rightarrow$h-$WO_3$ conversion.

The starting hexagonal structures collapsed in an exothermic reaction between 450–600°C and transformed into monoclinic WO_3. Thus for sensor and electrochromic applications our results showed that 1 was stable up to 450–500°C, while 2 and 2a were stable up to 400–450°C. Furthermore 2b was stable up to 500°C due to its high sodium content, which stabilized the hexagonal tungsten oxide structure better.

Upon further annealing, between 750-800°C monoclinic WO_3 transformed reversibly into tetragonal WO_3. Compared to 1, a separate feature of 2 was that from 700°C $Na_2W_4O_{13}$ was also detected, which was a result of the sodium content of 2. Above 700°C 2a and 2b showed small differences in the occurring heat effects, compared to 2.

Acknowledgments

The Authors are indebted to Péter Király (Institute of Structural Chemistry, Chemical Research Center of the Hungarian Academy of Sciences, Budapest, Hungary) for recording the ^{1}H-MAS-NMR spectra. The financial support of the GVOP-3.2.1.-2004-04-0210/3.0 project is acknowledged.

References

1 E. Lassner and W.-D. Schubert, Tungsten. Properties, Chemistry, Technology of the Element, Alloys, and Chemical Compounds, Kluwer Academic/Plenum Publishers, New York 1999.
2 C. G. Grandqvist, Handbook of Inorganic Electrochromic Materials, Elsevier, Amsterdam 1995.
3 M. Grätzel, Nature, 414 (2001) 338.
4 S. Wang, X. Feng, J. Yao and L. Jiang, Angew. Chem. Int. Ed., 45 (2006) 1264.
5 S. H. Baeck, T. Jaramill, G. D. Stucky and E. W. McFarland, Nano Lett., 2 (2002) 831.
6 I. Turyan, U. O. Krasovec, B. Orel, T. Saraidorov, R. Reinsfeld and D. Mandler, Adv. Mater., 12 (2000) 330.
7 C. Santato, M. Odziemkowski, M. Ulmann and J. Augustynski, J. Am. Chem. Soc., 123 (2001) 10639.
8 Y. He, Z. Wu, L. Fu, C. Li, Y. Miao, L. Cao, H. Fan and B. Zou, Chem. Mater., 15 (2003) 4039.
9 B. Xue, J. Peng, Z. Xin, Y. Kong, L. Li and B. Li, J. Mater. Chem., 15 (2005) 4793.
10 J. M. Ortega, A. I. Martinez, D. R. Acosta and C. R. Magana, Sol. Energy Mater. Sol. Cells., 90 (2006) 2471.
11 S. M. A. Durrani, E. E. Khawaja, M. A. Salim, M. F. Al-Kuhaili and A. M. Al-Shukri, Sol. Energy Mater. Sol. Cells., 71 (2002) 313.
12 J. Polleux, A. Gurlo, N. Barsan, U. Weimar, M. Antonietti and M. Niederberger, Angew. Chem. Int. Ed., 45 (2006) 261.
13 X. L. Li, T. J. Lou, X. M. Sun and Y. D. Li, Inorg. Chem., 43 (2004) 5442.
14 G. Shaw, I.P. Parkin, K. F. E. Pratt and D. E. Williams, J. Mater. Chem., 15 (2005) 149.
15 C. J. Jin, T. Yamazaki, Y. Shirai, T. Yoshiwaza, T. Kikuta, N. Nakatani and H. Takeda, Thin Solid Films, 474 (2005) 255.
16 A. Hoel, L. F. Reyes, S. Saukko, P. Heszler, V. Lantto and C. G. Granqvist, Sensor. Actuat. B, 105 (2005) 283.

17 C. Balázsi, A. K. Prasad, J. Pfeifer, A. L. Tóth and P. I. Gouma, SEMINANO2005 – First International Workshop on Seminconductor Nanocrystals, Budapest, Hungary 2005, Vol. 1, pp. 79–83. http://www.mfa.kfki.hu/conferences/seminano2005/pdf/p079_Balazsi_man.pdf
18 M. M. Natile, F. Tomaello and A. Glisenti, Chem. Mater., 18 (2006) 3270.
19 T. W. Bitner and J. I. Zink, Inorg. Chem., 41 (2002) 967.
20 A. M. Garrido Pedrosa, M. J. B. Souza, D. M. A Melo and A. S.Araujo, J. Therm. Anal. Cal., 87 (2007) 349.
21 T. Onfroy, G. Clet and M. Houlla, J. Phys. Chem. B, 109 (2005) 3345.
22 W. Han, M. Hibino and T. Kudo, Solid State Ionics, 128 (2000) 25.
23 O. Y. Khyzhun, Y. M. Solonin and V. F. Dobrovolsky, J. Alloys. Compd., 320 (2001) 1.
24 J. Pfeifer, C. Balázsi, B. A. Kiss, B. Pécz and A. L. Tóth, J. Mater. Sci. Lett., 18 (1999) 1103.
25 B. Gerand, G. Nowogrocki, J. Guenot and M. Figlarz, J. Solid State Chem., 29 (1979) 429.
26 Y. Oaki and H. Imai, Adv. Mater., 18 (2006) 1807.
27 Z. Gu, Y. Ma, W. Yang, G. Zhang and J. Yao, Chem. Commun., (2005) 3597.
28 Y. Wu, Z. Xi, G. Zhang, J. Yu and D. Guo, J. Cryst. Growth, 292 (2006) 143.
29 K. H. Cheng, A. J. Jacobson and M. S. Wittingham, Solid State Ionics, 5 (1981) 355.
30 B. Schlasche and R. Schöllhorn, Rev. Chim. Miner., 19 (1982) 534.
31 A. M. De La Cruz, L. M. Torres-Martínez, G. García-Alvaro, E. Morán and M. A. Alario-Franco, Solid State Ionics, 84 (1996) 181.
32 M. S. Wittingham, J. Li, J. D. Guo and P. Zavalij, Mater. Sci. Forum, 152–153 (1994) 99.
33 L. Seguin and M. Figlarz, Solid State Ionics, (1993) 437.
34 W. Han, M. Hibino and T. Kudo, B. Chem. Soc. Jpn., 71 (1998) 933.
35 N. Kumagai, N. Kumagai, Y. Umetzu, K. Tanno and J. P. Pereira-Ramos, Solid State Ionics, 86–88 (1996) 1443.
36 M. Figlarz, B. Dumont, R. Gerand and B. Beaudoin, J. Microsc. Spectrocs. Electron., 7 (1982) 371.
37 A. Al Mohammad and M. Gillet, Thin Solid Films, 408 (2002) 302.
38 O. Yamaguchi, D. Tomihisa, H. Kawabata and K. Shimizu, J. Am. Ceram. Soc., 70 (1987) C-94.
39 I. M. Szilágyi, F. Hange, J. Madarász and G. Pokol, Eur. J. Inorg. Chem., 17 (2006) 3413.
40 C. Balázsi and J. Pfeifer, Solid State Ionics, 151 (2002) 353.
41 J. Pfeifer, C. Guifang, P. Tekula-Buxbaum, B. A. Kiss, M. Farkas-Jahnke and K. Vadasdi, J. Solid State Chem., 119 (1995) 90.
42 D. G. Cory and W. M. Ritchey, J. Magn. Reson., 80 (1988) 128.
43 J. Madarász, I. M. Szilágyi, F. Hange and G. Pokol, J. Anal. Appl. Pyrolysis, 72 (2004) 197.
44 I. M. Szilágyi, J. Madarász, F. Hange and G. Pokol, J. Therm. Anal. Cal., 88 (2007) 139.
45 N. M. Laptash, S. A. Polyshchuk, E. I. Melnichenko and Y. Y. Kravtzova, J. Thermal. Anal., 39 (1993) 1477.

Received: June 12, 2007
Accepted: May 12, 2008
OnlineFirst: September 20, 2008

DOI: 10.1007/s10973-007-8601-y